AIAA JOURNAL
Vol. 38, No. 9, September 2000

# Quantitative Effects of Projectile-Launch Tube Wall Friction on Ballistic Range Operation

Akihiro Sasoh,* Shinji Ohba,† and Kazuyoshi Takayama‡
*Tohoku University, Sendai 980-8577, Japan*

**Theoretical and experimental studies are conducted on the quantitative evaluation of a friction force at the interface between a projectile and the launch tube wall in a ballistic range. From a mechanical balance relation applied to the projectile, the friction force is expressed theoretically as a function of the net acceleration of the projectile. With this formulation, experimentally measured in-bore projectile velocity profiles obtained using a velocity interferometer system for any reflector are well interpreted. If the initial projectile motion is significantly suppressed by the friction force while the burning rate of the propellant remains significant, the base pressure becomes much higher than that with a negligibly small friction force, thereby enhancing the net acceleration. However, if the projectile-tube fit is excessively high, the main function of the friction force is to decrease the muzzle velocity.**

## Nomenclature

$A$ = bore cross-sectional area, m$^2$
$a_f$ = deceleration due to friction force (negative value) [Eq. (22)], m/s$^2$
$a_n$ = net acceleration, m/s$^2$
$D_p$ = diameter of projectile, m
$D_t$ = diameter of launch tube, m
$E$ = Young's modulus of projectile, Pa
$F_b$ = force exerted on projectile due to base pressure, N
$F_f$ = friction force, N
$F_n$ = net force, N
$L_p$ = effective length of projectile, m
$m_p$ = projectile mass, kg
$p$ = pressure, Pa
$p_b$ = projectile base pressure, Pa
$p_R$ = statically measured diaphragm rupture pressure, Pa
$p_1$ = measured propellant chamber pressure, upstream, Pa
$p_2$ = measured propellant chamber pressure, near diaphragm, Pa
$r$ = radial coordinate, m
$S$ = projectile side wall area, m$^2$
$U_p$ = projectile speed, m/s
$x_p$ = projectile travel distance in launch tube, m
$z$ = axial coordinate on projectile frame, m
$z_c$ = the neutral location where $\sigma_r$ vanishes, m; see Eqs. (14) and (20)
$z_0$ = characteristic length on kinematic friction [Eq. (16)], m
$\alpha$ = thermal expansion coefficient of projectile, K$^{-1}$
$\beta$ = normal stress term related to inertia and material expansion [Eq. (17)], Pa
$\Delta T$ = temperature difference, K
$\Delta z$ = infinitesimal increment in $z$, m
$\epsilon$ = length fraction of contact [Eq. (21)]
$\mu$ = static friction coefficient
$\mu'$ = kinematic friction coefficient
$\nu$ = Poisson's ratio of projectile
$\xi$ = dimensionless excess diameter; Eq. (6)
$\rho_p$ = density of projectile, kg/m$^3$
$\sigma_r$ = normal stress in radial direction at projectile–wall interface, positive value corresponds to compression, Pa
$\sigma_z$ = normal stress in axial direction, positive value corresponds to compression

Received 8 April 1999; revision received 8 November 1999; accepted for publication 29 January 2000. 

*Associate Professor, Shock Wave Research Center, Institute of Fluid Science, 2-1-1 Katahira, Aoba-ku. Associate Fellow AIAA.
†Graduate Student, Shock Wave Research Center, Institute of Fluid Science, 2-1-1 Katahira, Aoba-ku; currently Engineer, JGC Company, Shin-Ohtemachi Building, Ohtemachi, Chiyoda-ku, Tokyo 100-0004, Japan.
‡Professor, Director, Shock Wave Research Center, Institute of Fluid Science, 2-1-1 Katahira, Aoba-ku. Senior Member AIAA.

## I. Introduction

BALLISTIC range technology is applicable over various fields. Currently, main subjects are on-ground super/hypersonic flight simulation[1–3] and hypervelocity impact studies.[4,5] Recently, related technologies even include medical applications, for example, needleless delivery of drugs in dry powder form to the skin or mucosal surfaces.[6] With these diversified applications, required specifications to the device are also diversified. There are many applications, for example, dynamic/mechanical property tests of solid specimen, in which a required muzzle velocity is modest, of the order of 1 km/s, other specifications are more important; in particular, in the modest muzzle velocity range, the accuracy in controlling the muzzle velocity is often most important.

In most cases, the fit of a projectile in a launch tube is an important parameter. On one hand, if the fit is too loose, the projectile may ballot in-bore or experience blow-by of the propellant gas. On the other hand, with an excessively tight fit the friction force causes a decrease in the muzzle velocity and/or serious wear of the tube and the projectile. There exists an optimum condition of the fit that depends on the expected function of a device. In high-muzzle-velocity guns, the effect of a drag force at the projectile–wall interface on the ballistic performance is mainly caused by engraving the projectile material during the early travel of the projectile in the launch tube;[7] after being engraved, the drag force usually becomes negligible.[8] However, with a modest muzzle velocity of the order of 1 km/s or lower, the friction force at the interface between the projectile and the smooth tube wall can significantly affect the performance of a range.

For nonrifled ballistic ranges, in previous studies the typical treatment is that the friction force is simply estimated from experimentally measured, facility-dependent characteristics[9,10] or is neglected.[11] Quantitative estimation of the friction force in modest-muzzle-speed ballistic range still warrants further investigations.[9,12] To the best knowledge of the authors, a wall-friction model developed by Groth and Gottlieb[13] and Matsumura et al.[14] is so far the most sophisticated. Their model is constructed based on one-dimensional, quasi-steady-state elastic relations applied to the projectile. In spite of their detailed analysis, the significant effect of the projectile–launch tube wall friction force on ballistic range operation did not appear in their experiments; further investigations are still necessary to validate their model experimentally.

For rifled barrels, a study on the projectile sliding force was done.[15] However, the condition is much different from that for nonrifled ones; the results of the study are not directly applicable to smooth-bore guns.

The purpose of this study is to develop and to validate experimentally a general formula on the projectile–tube wall friction force applicable to a modest-muzzle-speed, smooth-bore ballistic range, where the effect of the engraving is not taken into account and to discuss its effects on range performance.

## II. Kinematic Friction Model

The present model is similar to Groth and Gottlieb's model.[13] In their paper, a friction force is not presented in a closed form. In this study, with minor simplifications, a friction force and a projectile base pressure will be given in a closed form. Figure 1 schematically illustrates a mechanical relation on a projectile, $L_p$ in length, which is being accelerated in the launch tube of a ballistic range. In the present analysis, a force in the positive-$z$ direction has a positive value. The projectile experiences a mechanical force $F_b$ on its base due to the burnt gas of the propellant. If a normal force exists at the interface between the tube wall and the projectile, a friction force $F_f$ (negative value) is generated in the opposite direction of the velocity. The net force $F_n$ is calculated as the resultant force. These relations are expressed by the following equations:

$$F_b = \int_{\text{base}} p \, \mathrm{d}A \tag{1}$$

$$F_f = -\int_{\text{side}} \mu' \sigma_r \, \mathrm{d}S \le 0 \tag{2}$$

$$F_n = F_b + F_f \tag{3}$$

where $p$, $\sigma_r$, and $\mu'$ designate the pressure on the projectile base, a radial stress on the launch tube wall, and the kinematic friction coefficient between the projectile and the wall, respectively. In this paper, a positive value of $\sigma$ corresponds to compression. The net acceleration of the projectile is given by

$$a_n = F_n / m_p \tag{4}$$

The mechanical balance in the infinitesimal segment of the projectile between $z$ and $z + \Delta z$ is considered. A sabot is not used to back the projectile; the projectile can be in direct contact with the tube wall. It is assumed that each strain is within the corresponding elastic limit. The net acceleration $a_n$ is assumed to be uniform over the projectile. This assumption is equivalent to neglecting stress waves in the projectile. That is, the projectile is assumed to be in mechanical equilibrium on the frame attached to the projectile. Ambient gaseous pressure around the projectile is neglected. Hooke's law for elastic deformation of the projectile is expressed by[13,14]

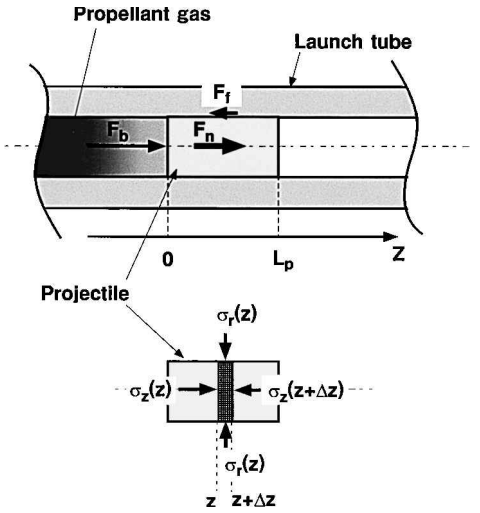


**Fig. 1 Dynamic relation on ballistic range projectile.**

$$\sigma_r(z) = \begin{cases} \dfrac{E}{1-\nu}\left(\dfrac{\xi}{\xi+1} + \dfrac{\nu\sigma_z(z)}{E} + \alpha\Delta T\right), & \text{for} \quad \sigma_r > 0 \\ 0, & \text{elsewhere} \end{cases} \tag{5}$$

$$\xi \equiv (D_p - D_t)/D_t \tag{6}$$

In Eq. (5) $\sigma_z$ is a normal stress in the axial direction. A compression stress is defined to be positive. Both $\sigma_r$ and $\sigma_z$ are functions of $z$, and $\xi$ is a dimensionless excess diameter of the projectile measured without any mechanical/thermal deformation.

The equation of motion applied to the control volume is given by

$$\rho_p a_n = -\frac{\mathrm{d}\sigma_z(z)}{\mathrm{d}z} - \frac{4\mu'\sigma_r(z)}{D_t} \tag{7}$$

where $\rho_p$ is the density of the projectile. The following analysis is applicable only for $a_n > 0$. As long as the projectile is in full contact with the launch tube wall, the present model can be applied even to cases of $a_n < 0$. Although not presented in this paper, a general formulation for $a_n < 0$ is easily done.

The boundary conditions on $\sigma_z$ are as follows:

$$\sigma_z(0) = p_b \tag{8}$$

$$\sigma_z(L_p) = 0 \tag{9}$$

In Eq. (8), $p_b$ is a gaseous pressure exerting on the base of the projectile. $L_p$ is the effective length of the projectile. The friction force $F_f$ is obtained as a Lebesque integration of Eq. (5) multiplied by a kinematic friction coefficient $\mu'$:

$$F_f = -\mu' \int_{\sigma_r \ge 0} \sigma_r(z) \pi D_t \, \mathrm{d}z \tag{10}$$

and $\mu'$ is assumed to be a constant.

Here, as in many laboratory applications, the effect of viscous shear force due to the fluid layer between the projectile and the tube wall is neglected. There are three situations for the contact between the projectile and the launch tube wall.

1) No contact is where the projectile is not in contact with the launch tube wall at all:

$$F_f = 0 \tag{11}$$

The integration of Eq. (7) with $\sigma_r = 0$ and Eq. (9) yields

$$\sigma_z(z) = \rho_p a_n (L_p - z), \qquad 0 \le z \le L_p \tag{12}$$

Therefore, from Eq. (8),

$$p_b = \rho_p a_n L_p \tag{13}$$

2) Partial contact is where a fraction of the projectile side surface is in contact with the launch tube wall. Here, let the neutral location where $\sigma_r$ vanishes be $z_c$. It is obtained by substituting Eq. (12) for Eq. (5) with $\sigma_r = 0$:

$$z_c = L_p + (E/\rho_p a_n \nu)[\xi/(\xi+1) + \alpha\Delta T], \quad \text{for} \quad 0 < z_c < L_p \tag{14}$$

In the region $0 \le z \le z_c$, Eq. (7) is solved with Eqs. (5) and (8):

$$\sigma_z(z) = (p_b + \beta)e^{-(z/z_0)} - \beta \tag{15}$$

$$z_0 = \frac{(1-\nu)D_t}{4\nu\mu'} \tag{16}$$

$$\beta = \rho_p z_0 a_n + (E/\nu)[\xi/(\xi+1) + \alpha\Delta T] \tag{17}$$

where $p_b$ is expressed in a closed form by equating Eqs. (12) and (15) at $z = z_c$:

$$p_b = \rho_p a_n (L_p - z_c) e^{z_c/z_0} + \left(e^{z_c/z_0} - 1\right)\beta \tag{18}$$

$F_f$ is calculated, using Eqs. (5), (15), (17), and (18), by applying Eq. (10) to a region $0 \le z \le z_c$:

$$F_f = -\frac{\pi \nu \mu' D_t z_0}{1-\nu}\left[\frac{E}{\nu}\left(\frac{\xi}{\xi+1}+\alpha\Delta T\right)\left(e^{z_c/z_0}-1\right) + \rho_p a_n\left\{(L_p+z_0)\left(e^{z_c/z_0}-1\right)-z_c e^{z_c/z_0}\right\}\right] \tag{19}$$

3) Full contact is where the whole side of the projectile is in contact with the launch tube wall. In this case, $p_b$ and $F_f$ are obtained by substituting $z_c = L_p$ for Eqs. (18) and (19), respectively.

To summarize these results, Eqs. (18) and (19) become applicable to any contact condition by redefining $z_c$ such that

$$z_c = \begin{cases} 0, & \epsilon \le 0 \quad \text{(no contact)} \\ \epsilon L_p, & 0 < \epsilon < 1 \quad \text{(partial contact)} \\ L_p, & 1 \le \epsilon \quad \text{(full contact)} \end{cases} \tag{20}$$

$$\epsilon \equiv 1 + \frac{E}{\rho_p a_n L_p \nu}\left(\frac{\xi}{\xi+1}+\alpha\Delta T\right) \tag{21}$$

## III. Experimental Apparatus

Ballistic range operation experiments were conducted using a single-stage gun. The bore diameter and the length of the launch tube are 25 mm and 2.0 m, respectively. The launch tube is connected to a test chamber, which was evacuated to a pressure lower than 100 Pa before a shot. By substitution of typical values, a projectile velocity of $10^3$ m/s, the speed of sound of the ambient gas of 340 m/s, and a specific heat ratio of 1.4, for the shock relations, the pressure on the projectile frontal surface is calculated to be 1.7 kPa. This value is four orders in magnitude smaller than the peak value level of the projectile base pressure. Therefore, the frontal surface force is negligible in estimating the acceleration of the projectile. The test chamber has a pair of 300-mm-diam acrylic windows. The propellant chamber (Fig. 2) has an inner diameter of 35 mm and a length of 113 mm. A hydroxylammoniumnitrate (HAN)-based liquid propellant, LP1846,[16] was used as the main propellant. The propellant was bulk loaded. The shot-to-shot scatter in the muzzle velocity was ±3% (Ref. 17). The liquid propellant was ignited by 0.9-g double-based smokeless powder, which in turn was ignited using an electrical igniter. The propellant chamber was diaphragmed by a layer of stainless steel disk. Its static rupture pressure was controlled by varying the thickness of the disk and/or the depth of the pressed cross grooves on its surface. The time variation of pressures $p_1$ and $p_2$ in the propellant chamber were measured by two recess-mounted piezoelectric pressure tranceducers, the rise time of which was 1 $\mu$s. The accuracy in the pressure measurement was better than ±2%.

Figure 3 shows the configuration of the projectile. It configures as a cylinder with a Bridgman seal employed on its base. It is made of high-density polyethylene. The specifications of its properties are given in Table 1. The mass of the projectile was 16.1 g ± 2%. To vary the fit to the launch tube, the diameter of the projectile $D_p$, at a room temperature, was varied from 24.92 to 25.14 mm; the launch tube diameter was 25.00 mm. A sabot is not used in this study.

The in-tube velocity history of the projectile was measured using a velocity interferometer system for any reflector (VISAR)[18,19] (Fig. 4). A 514.5-nm wavelength light beam from a 2-W argon ion laser is introduced to the test chamber and incident on the front surface of the projectile. A retroreflective sheet (3970G, 3M) on the projectile surface directs the reflected beam in exactly same direction as that of the incident beam. After leaving the test chamber, the reflected beam is introduced to the VISAR. After transmitting

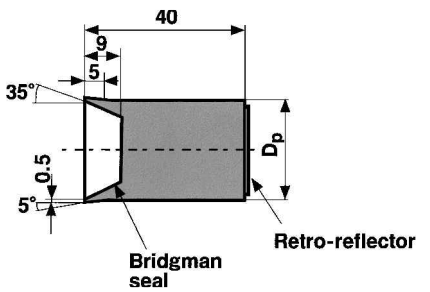


**Fig. 3 Projectile configuration; length in millimeters.**

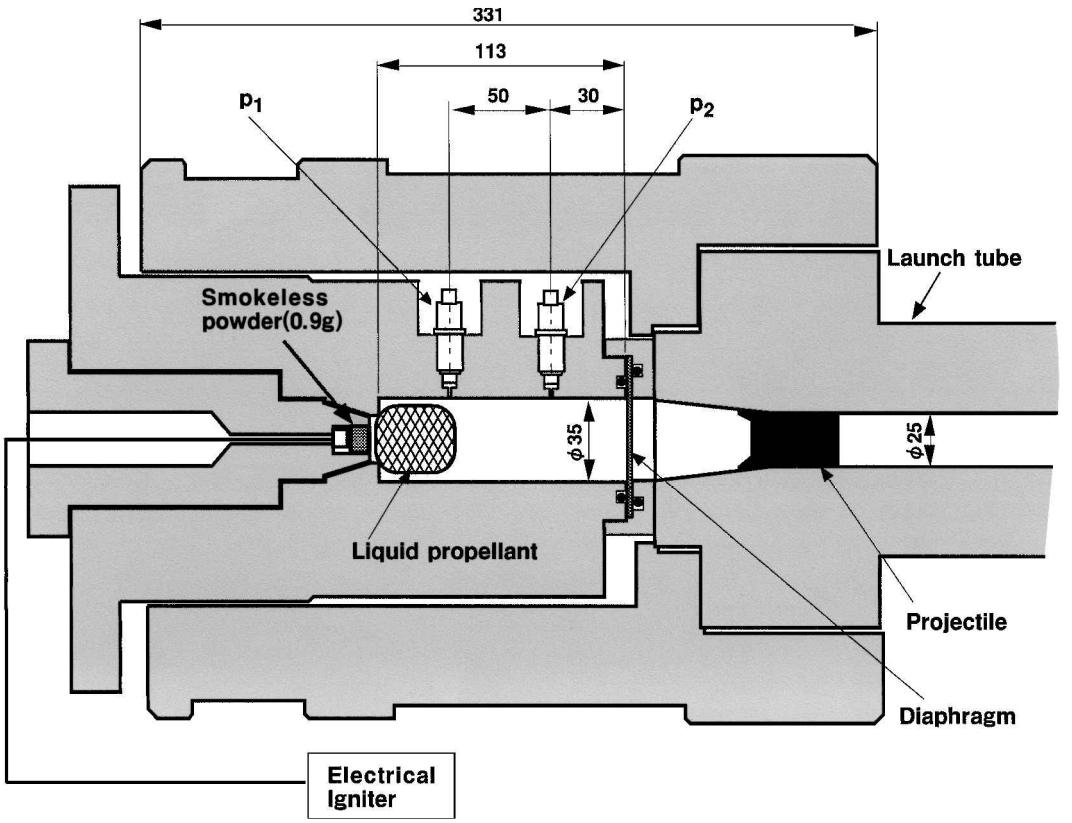


**Fig. 2 Schematic of propellant chamber; length in millimeters.**

**Table 1 Properties of projectile material**

| Parameter | Value |
|---|---|
| Density | $9.4 \times 10^2$ kg/m$^3$ |
| Tensile stress | 31 MPa |
| Young's modulus | 774 MPa |
| Thermal expansion coefficient | $2.0 \times 10^{-4}$ K$^{-1}$ |
| Poisson's ratio[a] | 0.458 |

[a]No data for this particular product are available; typical value for polyethylene is employed.

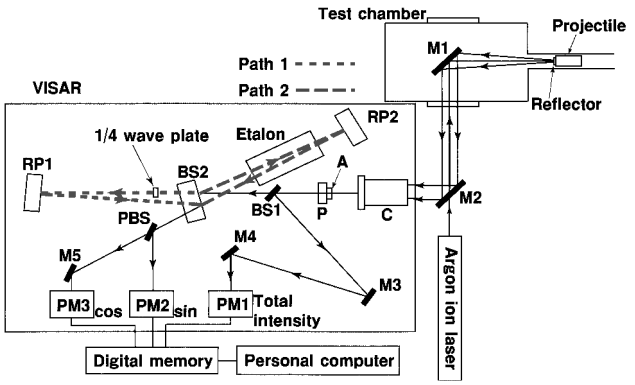


**Fig. 4 VISAR arrangement: A, aperture; BS, beam splitter; C, collimator; M, mirror; P, polarizer; PM, photomultiplier, and RP, reflection prism.**

through the polarizer (P), the beam is partially split by the beam splitter 1 (BS1), and sensed by the photomultiplier 1 (PM1). The sensed intensity scales with the total intensity of the beam and is utilized to normalize the intensities of interferometric beams. The beam transmitting through BS1 is split into two. One is circular modulated and reflected back from the reflection prism 1 (RP1) (path 1). The other returns from RP2, propagates through a longer optical path (path 2). The two beams interfere with each other on BS2. The intensities of orthogonal components of the interfered beam are continuously measured by PM2 and PM3. In this device, the fringe constant is in proportion with the reciprocal of the difference in the optical length between the paths 1 and 2, which is controlled by the thickness of the etalon. In this study, the fringe constant was set to 130.84 m/s. The measured signals were recorded in a data acquisition system and numerically analyzed by a personal computer. The sampling rate of the data acquisition was set to 10 $\mu$s. The accuracy in the velocity measurement was better than $\pm 1$ m/s. The corresponding accuracies in determining the position and acceleration of the projectile were $\pm 1$ and $\pm 2\%$, respectively.

## IV. Results and Discussion

### A. Measurement of Friction Coefficients

The static and kinematic friction coefficients were experimentally measured using the same gun by observing the motion of a projectile driven by high-pressure nitrogen, which was supplied behind the projectile through the propellant chamber. In this measurement, the igniter cartridge was replaced with an appropriate pneumatic feedthrough. The speed of the projectile was kept lower than 1 m/s. Because of this low-velocity level, the pressure on the base of the projectile was estimated with an accuracy of better than $10^{-3}\%$ by the pressure measured in the propellant chamber. The effect of the pressure on increasing the radial stress on the tube wall was negligible. The radial force was determined through Eq. (5) with $\sigma_z = 0$. The experiments were conducted by varying $\xi$ and $\Delta T$. From a pressure with which the projectile began to move, the static friction coefficient $\mu$ was determined. From a pressure at which the projectile coasted in the tube at a constant low speed, the kinematic friction coefficient $\mu'$ was determined. From the measurements, the values of $\mu$ and $\mu'$ were determined to be 0.19 and 0.10, respectively; the corresponding accuracies were both $\pm 3\%$.

### B. Effects on Acceleration Performance

Figures 5a–5d show projectile acceleration characteristics measured with a liquid propellant mass of 15 g and a static diaphragm

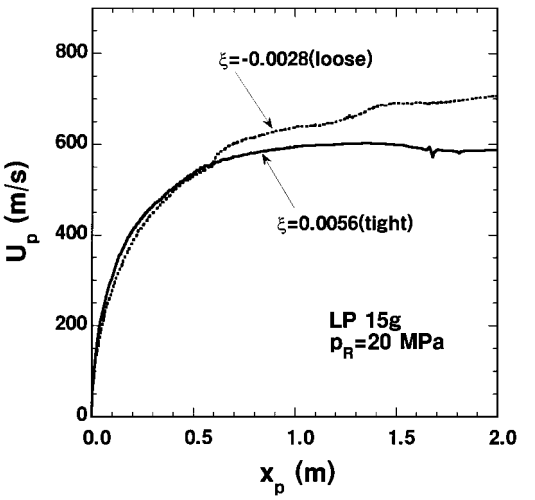


a) $U_p$ (projectile speed) vs $x_p$

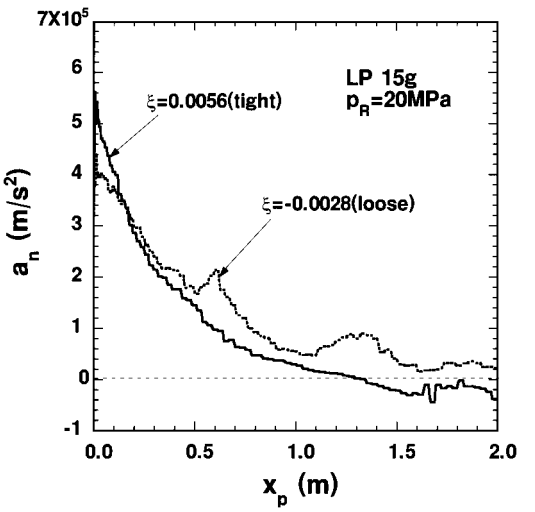


b) $a_n$ vs $x_p$

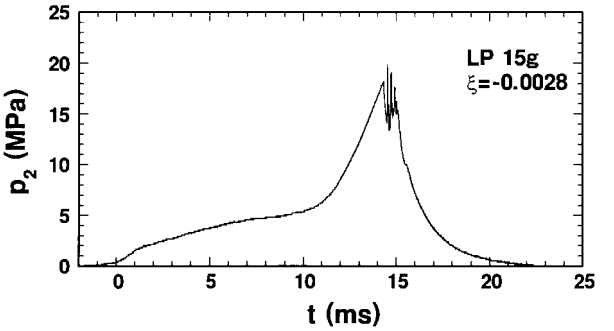


c) Time variation of $p_2$ (loose fit, $\xi = -0.0028$)

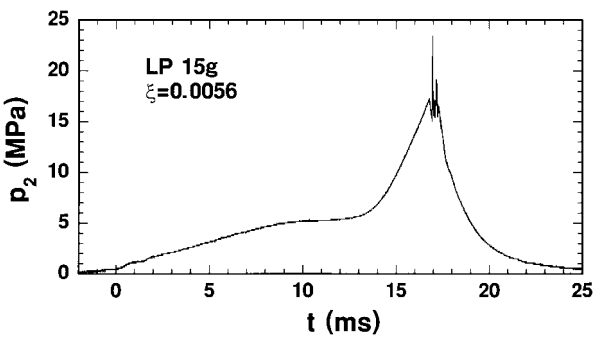


d) Time variation of $p_2$ (tight fit, $\xi = 0.0056$)

**Fig. 5 Measured acceleration characteristics with different $\xi$: 15-g liquid propellant.**

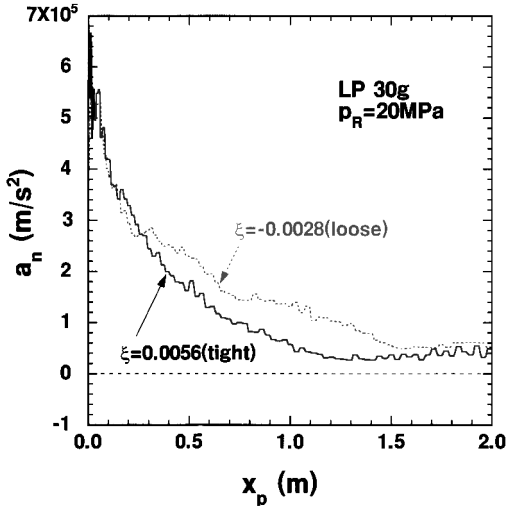


a) $a_n$ vs $x_p$

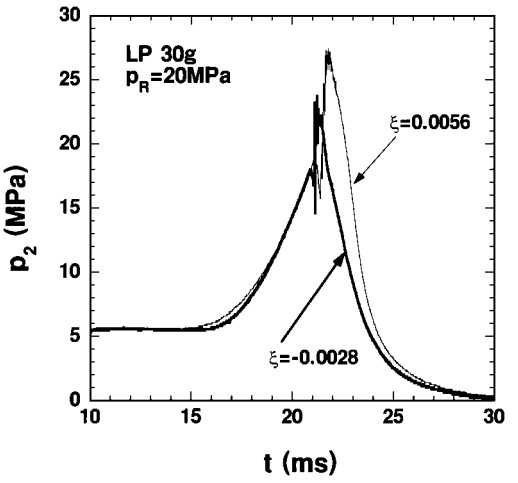


b) Time variations of $p_2$

**Fig. 6 Measured acceleration characteristics with different $\xi$: 30-g liquid propellant.**

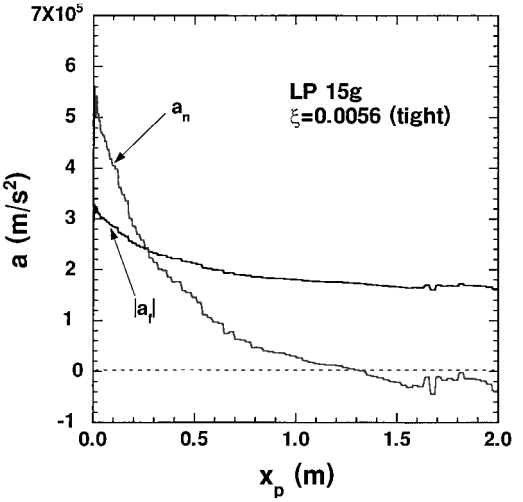


a) 15-g liquid propellant

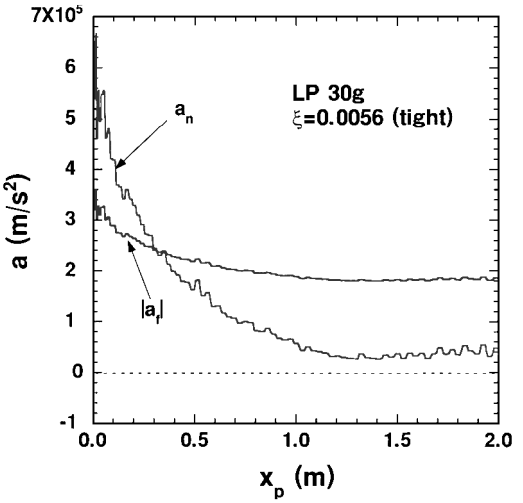


b) 30-g liquid propellant

**Fig. 7 Projectile acceleration profile: tight fit ($\xi = 0.0056$), $p_R = 20$ MPa ± 15%.**

rupture pressure of 20 MPa ±15%. Acceleration $a_n$ (Fig. 5b) was calculated by smoothing the experimentally measured $U_p$ profile (Fig. 5a) and time differentiating it. Here, the projectile travel distance, which is obtained by numerically integrating the $U_p$–$t$ profile, is denoted by $x_p$. A loose fit condition is represented by $\xi = -0.0028$. In this case, the initial diameter of the projectile loaded in the launch tube is smaller than the inner diameter of the launch tube by 0.28%. The burnt gas is sealed only by the Bridgman seal on the base. The friction force due to the Bridgman seal is estimated to be negligible. A tight fit condition is represented by $\xi = 0.0056$. In this case, the projectile was prerefrigerated so that it was smoothly loaded in the launch tube.

The propellant chamber pressure histories (Figs. 5c and 5d) exhibit some characteristics peculiar to the liquid propellant. Before a rapid rise in $p_2$ just before the diaphragm rupture, it gradually increases and keeps an almost constant value. This constant value is almost equal to the value that is attained only with the smokeless powder.[17] This flat pressure profile is believed to be caused by the pyrolysis of the liquid propellant. After maintaining this low pressure for about 10 ms, the pressure begins to rise relatively rapidly. This relatively steep rise in pressure is due to the combustion of the propellant.

As seen in Fig. 5b, in each case $a_n$ is highest right after the diaphragm rupture. Traveling over less than 20% of the total length of the launch tube, $a_n$ drops to the half of the peak value. It is interesting that the peak value is larger with the tight fit ($\xi = 0.0056$). This tendency is better interpreted by carefully analyzing the measured propellant chamber pressures as shown in Figs. 5c and 5d. The pressure on the projectile base is affected by the relation between the propellant gas generation rate and the motion of the projectile. After the diaphragm is ruptured, the projectile motion causes expansion waves propagating through the burnt propellant gas, thereby decreasing the projectile base pressure. However, if the propellant burning rate is significant even after the diaphragm rupture, the base pressure can continue to increase. In the present experimental condition, the liquid propellant continues to burn even when/after the diaphragm is ruptured. With the tight fit the initial projectile motion is suppressed by a large friction force, thereby keeping the base pressure relatively high due to on-going propellant combustion. Note that the effective diaphragm rupture pressure evaluated by the experimentally measured $p_2$ are 18.2 MPa for $\xi = -0.0028$ and 17.3 MPa for $\xi = 0.0056$. With the loose fit (Fig. 5c), the measured pressure abruptly decreased by about 5 MPa due to the diaphragm rupture. On the other hand, with the tight fit, the corresponding pressure drop was less than 2 MPa; the pressure almost recovered once again. As a result, $a_n$ became higher even with the larger friction force though the effective diaphragm rupture pressure was slightly lower.

A similar tendency was observed when the liquid propellant mass was doubled (Fig. 6). In this case, the propellant chamber pressure overshot after the diaphragm rupture (Fig.6 b). The overshot value was much larger with the tight fit ($\xi = 0.0056$), yielding a value of $a_n$ comparable with that of the loose fit. However, with the tighter fit $a_n$ is much decreased near the muzzle; for the smaller propellant mass (Fig. 5b), the projectile was even decelerated near the muzzle.

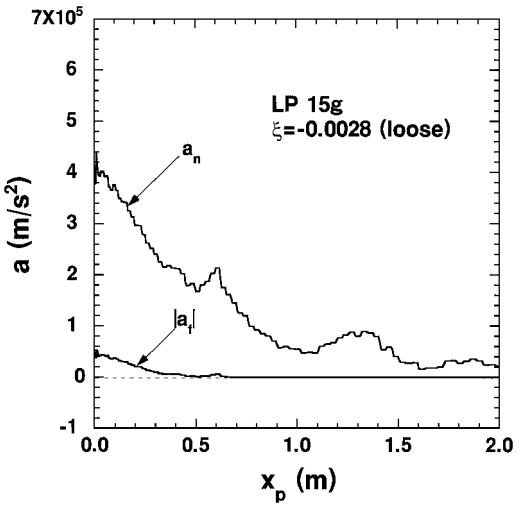


a) 15-g liquid propellant

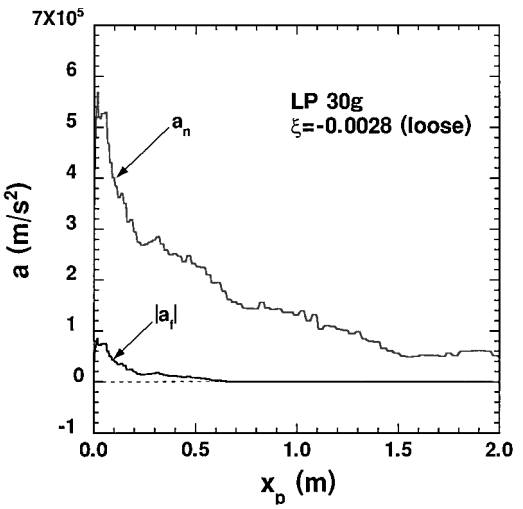


b) 30-g liquid propellant

**Fig. 8 Projectile acceleration profile: loose fit ($\xi = -0.0028$), $p_R = 20$ MPa ± 15%.**

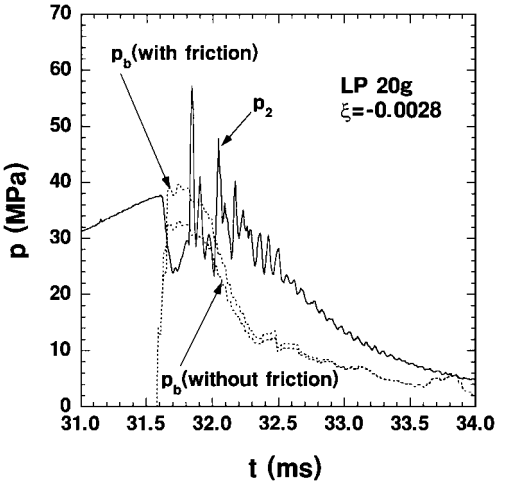


a) 20-g liquid propellant

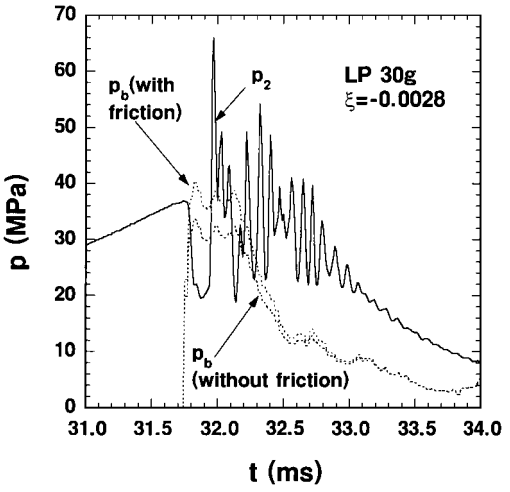


b) 30-g liquid propellant

**Fig. 9 Time variation of $p_b$ and $p_2$: $p_R = 40$ MPa ± 10%.**

As a result, in the present study, the muzzle velocity always became lower with the tighter fit.

### C. Quantitative Significance

A deceleration due to the friction force (negative value) $a_f$ is defined by

$$a_f = F_f / m_p \tag{22}$$

where $F_f$ has a negative value and is calculated from a measured $a_n$ profile using Eq. (10). Figures 7a and 7b show in-tube acceleration profiles with the tight fit. At $x_p = 0$, the absolute value of the deceleration due to friction $|a_f|$ becomes higher than the half of $a_n$. Traveling down in the launch tube, the net acceleration decreases rapidly. The variations of $|a_f|$ are relatively small. As a result, at $x_p > 0.3$ m, $|a_f|$ becomes higher than $a_n$. With 15-g liquid propellant, $a_n$ becomes negative at $1.3 \leq x_p \leq 2.0$. This tendency results in a lower muzzle speed with the excessively tight fit.

In the case of the loose fit ($\xi = -0.0028$) $|a_f|$ has a positive value only at $x_p < 0.7$ m (Fig. 8). Even in this location, $|a_f|$ becomes only 10% of $a_n$ at most. In these cases, the effect of the friction force on the ballistic range performance is negligibly small.

To validate the present friction model quantitatively, it is desirable that $p_b$ could be independently measured. However, technically the direct measurement of $p_b$ all through the projectile acceleration process is quite difficult. In place of the direct measurement, the following analyzes are made. Figures 9a and 9b show the time variation of pressure in the propellant chamber $p_2$, which was directly measured, and projectile base pressures $p_b$. Here $p_b$ are calculated from the measured $a_n$ profile: $p_b$ with a friction force is calculated using Eq. (18), and $p_b$ without a friction force is calculated using Eq. (13). The effective length of a projectile is calculated by dividing a projectile mass by the product of its cross-sectional area and density. This implies that the projectile is modeled as a solid cylinder. Because the pressure rise rate with the liquid propellant under the present conditions is modest, the diaphragm rupture pressure is well estimated as the peak value of $p_2$ at $t = 31.6$ μs in Fig. 9a and at $t = 31.7$ μs in Fig. 9b. In both cases, if $p_b$ is estimated without taking the friction into consideration, its value becomes lower than $p_2$. The error is from 10 to 20%. With the friction force, however, the value becomes reasonably close to $p_2$, within small fluctuations in the calculated $p_b$. From these results, it follows that by taking the contribution of the projectile–wall friction force into account, the projectile base pressure is much better estimated. Also the results of Fig. 9 suggest that even with the loose fit the effect of the friction force can be significant when $a_n$ is high.

## V. Conclusions

The friction force at the interface between a projectile and a smooth launch tube wall is expressed in a closed form as a function of the net acceleration of the projectile. Using a VISAR, projectile acceleration profiles were accurately measured with different fit tightnesses. In the case of the tight fit, the friction force can become comparable with the driving force made by the propellant gas. If the propellant burning rate is significant when the diaphragm is ruptured, with a large friction force the net acceleration slightly after the diaphragm rupture can once become even higher than that with the loose fit. This gain can be expected only during the beginning stage

of the acceleration; with excessively tight fit, the muzzle velocity becomes lowered. As is shown in Fig. 9, even if the fit is loose, the effects of the friction force on the acceleration profile can be significant if the net acceleration is high. The observed mechanical relation in the beginning stage of acceleration becomes consistent only by taking into account the friction force based on the present model. The present model can be useful as a modification of a simpler model where the friction force is assumed to be constant, in particular, in conducting better numerical simulation of ballistic range operation.

## Acknowledgments

Special thanks are due to Asahi Chemical Industry Company, Ltd., Oita, Japan, for supplying us with the liquid propellant. The authors are gratefulto E. Zaretsky, Ben-Gurion University, Israel, for his essential assistance in preparing for the velocity interferometer system for any reflector measurement and to T. Ito, Institute of Fluid Science, Tohoku University, for valuable discussions on the projectile friction model. Also the authors appreciate technical support from O. Onodera, H. Ojima, H. Ogawa, M. Adachi, K. Takahashi, N. Ito, and M. Kato.

## References

[1]Canning, T. N., Seiff, A., and James, C. S., "Ballistic-Range Technology," AGARDograph 138, Aug. 1970.

[2]Klingenberg, G., Knapton, J. D., Morrison, W. F., and Wren, G. P., *Liquid Propellant Gun Technology*, Vol. 175, Progress in Astronautics and Aeronautics, AIAA, Reston, VA, 1997, Chap. 2.

[3]Nonaka, S., Mizuno, H., and Takayama, K., "Ballistic Range Measurement of Shock Shapes in Intermediate Hypersonic Regime," AIAA Paper 99-1025, 1999.

[4]Fowles, G. R., Duvall, G. E., Asay, J., Bellamy, P., Feistmann, F., Grady, D., Michaels, T., and Mitchell, R., "Gas Gun for Impact Studies," *Review of Scientific Instruments*, Vol. 41, No. 7, 1970, pp. 984–997.

[5]Bourne, N. K., Rosenberg, Z., Johnson, D. J., Field, J. E., Timbs, A. E., and Flaxman, R. P., "Design and Construction of the UK Plate Impact Facility," *Measurement Science and Technology*, Vol. 10, No. 6, 1995, pp. 1462–1470.

[6]Bellhouse, B. J., Quinlan, N. J., and Ainsworth, R. W., "Needle-Less Delivery of Drugs, in Dry Powder Form, Using Shock Waves and Supersonic Gas Flow," *Shock Waves*, Vol. 1, Panther, Fyshwick, Australia, 1997, pp. 51–56.

[7]Krier, H., and Adams, M. J., "An Introduction to Gun Interior Ballistics and a Simplified Ballistic Code," *Interior Ballistics of Guns*, Vol. 66, Progress in Astronautics and Aeronautics, AIAA, New York, 1979, pp. 1–36.

[8]Seigel, A. E., "Theory of High-Muzzle-Velocity Guns," *Interior Ballistics of Guns*, Vol. 66, Progress in Astronautics and Aeronautics, AIAA, New York, 1979, pp. 135–175.

[9]Celminš, A. K., "Mathematical Modeling of Recoilless Rifle Interior Ballistics," *Interior Ballistics of Guns*, Vol. 66, Progress in Astronautics and Aeronautics, AIAA, New York, 1979, pp. 113–134.

[10]Bicen, A. F., Khezzar, L., and Whitelaw, J. H., "Subsonic Single-Phase Flow in a Gun Simulator," *AIAA Journal*, Vol. 25, No. 1, 1988, pp. 47–51.

[11]Kamimoto, G., Tsukamoto, A., and Otsuji, K., "Studies on Hypervelocity Model Launcher," Dept. of Aeronautical Engineering, Current Papers C.P. 34, Kyoto Univ., Japan, 1972.

[12]Baer, P. G., "Practical Interior Ballistic Analysis of Guns," *Interior Ballistics of Guns*, Vol. 66, Progress in Astronautics and Aeronautics, AIAA, New York, 1979, pp. 37–66.

[13]Groth, C. P. T., and Gottlieb, J. J., "Numerical Study of Two-Stage Light-Gas Hypervelocity Projectile Launchers," Inst. for Aerospace Studies, Univ. of Toronto, UTIAS Rept. 327, Toronto, ON, Canada, June 1988.

[14]Matsumura, T., Inoue, O., Gottlieb, J. J., and Takayama, K., "A Numerical Study of the Performance of a Two-Stage Light-Gas Gun," Inst. of Fluid Science Rept., Tohoku Univ., Sendai, Japan, Vol. 1, 1990, pp. 121–133.

[15]Stiffler, A. K., "Projectile Sliding Forces in a Rifled Barrel," *International Journal of Mechanical Sciences*, Vol. 25, No. 2, 1983, pp. 105–119.

[16]Klingenberg, G., Knapton, J. D., Morrison, W. F., and Wren, G. P., *Liquid Propellant Gun Technology*, Progress in Astronautics and Aeronautics, Vol. 175, AIAA, Reston, VA, 1997, Chaps. 4 and 8.

[17]Sasoh, A., Ohba, S., and Takayama, K., "Investigation on Utilization of Liquid Propellant in Ballistic Range Experiments," *Journal of Japan Explosive Society* (Kaya Ku Gakkaishi), Vol. 60, No. 5, 1999, pp. 205–211.

[18]Barker, L. M., and Hollenbach, R. E., "Laser Interferometer for Measuring High Velocities of Any Reflecting Surface," *Journal of Applied Physics*, Vol. 43, No. 11, 1972, pp. 4669–4675.

[19]Munson, D. E., and May, R. P., "Interior Ballistics of a Two-Stage Light Gas Gun Using Velocity Interferometry," *AIAA Journal*, Vol. 14, No. 2, 1976, pp. 235–242.

J. C. Hermanson
*Associate Editor*